FULL PAPER

ADVANCED FUNCTIONAL MATERIALS

Photoreplicated Anisotropic Liquid-Crystalline Lenses for Aberration Control and Dual-Layer Readout of Optical Discs

By *Henk R. Stapert*,* *Sergio del Valle*, *Emile J. K. Verstegen*, *Bianca M. I. van der Zande*, *Johan Lub* and *Sjoerd Stallinga*

This work describes the functional characterization of novel photoreplicated anisotropic lenses obtained from molds with different curvatures. These lenses were prepared by the photopolymerization of mixtures of a reactive liquid-crystalline bisacrylate and non-reactive derivatives of liquid-crystalline cyanobiphenyl. The phase diagrams, the polymerization kinetics as a function of temperature, and the birefringence as a function of temperature for various mixtures were determined. For the fabrication of lenses, the average liquid-crystal (LC) director of the mixtures has to be aligned in a single direction. Photoalignment and rubbing techniques were investigated to create a monodomain of the reactive material. Finally, optimal mixtures were used for the fabrication of anisotropic lenses. Aberrations were below 20 mλ root mean square (rms), which makes these LC lenses interesting for application in light paths, for example, as spherical aberration correction devices for dual- (or multiple-) layer optical storage.

1. Introduction

The ever-increasing demand for storage capacity on inexpensive removable media is a key driver behind the developments in the field of optical disc storage. The Blu-ray Disc (BD) format, with a capacity of around 25 GB, has recently been proposed as a successor to the Compact Disc (CD, 650 MB capacity) and Digital Versatile Disc (DVD, 4.7GB capacity).[1,2] This increase in capacity is made possible by the small wavelength of blue semiconductor lasers diodes ($\lambda = 405$ nm), and by the large numerical aperture ($NA = 0.85$) of the scanning objective lens ($NA = m \sin\alpha$, where α is the semi-angle of the cone of light emanating from the lens). These numbers result in a relatively small focal spot, with a diameter of roughly λ/NA, allowing the error-free readout of the smaller sized marks in the information layer of the disc.

A further increase in storage capacity can be obtained by increasing the number of information layers per disc. For example, a dual-layer BD-disc has two information layers separated by a 25 μm-thick spacer layer. This poses a problem for the BD-format, as the cone of light has to travel through the spacer layer when focusing on the second information layer. This introduces so-called spherical aberration, the phenomenon where the rays close to the axis of the converging cone of light have a different focal point than the rays on the outside of the cone. It results in a blurring of the focal spot and the loss of fidelity in the readout of the disc. The sensitivity to spherical aberration decreases with wavelength and increases with NA, by a power of four for small NA and even faster for moderate to large NA.[3]

The spherical aberration sensitivity is defined as the root-mean-square (rms) deviation of the wavefront of the converging cone from the ideal spherical wavefront, divided by the thickness of the spacer layer. It is still possible to readout information when the rms wavefront aberration is below approximately 0.072 waves, or 72 mλ[4] In such a case we say that the focal spot is "diffraction limited". For BD dual-layer discs, the 25 μm spacer layer introduces a 255 mλ rms spherical aberration, which is well beyond the diffraction limit. Clearly, in order for BD dual-layer to work this additional amount of spherical aberration must be compensated. There were similar problems with CD/DVD compatibility (trying to readout CDs with a DVD optical pick-up) where there is a mismatch in the CD and DVD formats causing spherical aberration. Different solutions for both situations have been proposed, such as an objective ($NA = 0.6$) with a liquid-crystal (LC) shutter,[5] dual objective actuators,[6] a dual focusing lens with a holographic optical element,[7] and LC microlenses.[8–10] These solutions all suffer from one or more drawbacks, such as slow switching speed, high sensitivity for skewness, high aberrations, or difficult processing. To enable dual-layer readout and backward compatibility with minimal spherical aberration, we propose a polarization-sensitive lens (PS lens) and a light path for optical readout of dual-layer discs.[11]

A PS-lens as shown in Figure 1 is made of a glass plate with refractive index n_g and a curved LC polymer surface with a curvature radius R. For the extraordinary (subscript e) and ordinary (subscript o) mode we find focal lengths: $f_e = R/(n_e - n_g)$ and $f_o = R/(n_o - n_g)$. When the lens is made by photoreplication n_g becomes 1, the refractive index of air. The amount of spherical aberration of the beam exiting the objective lens can be controlled by the vergence of the beam entering the objective

[*] Dr. H. R. Stapert, S. del Valle,[+] E. J. K. Verstegen, Dr. B. M. I. van der Zande, Dr. J. Lub, Dr. S. Stallinga
Philips Research Laboratories
Prof. Holstlaan 4, 5656 AA, Eindhoven, The Netherlands
e-mail: henk.stapert@philips.com
[+] Current address: EEIGM, 6, Rue Bastien Lepage, Nancy, France.

  DOI: 10.1002/adfm.200304385 *Adv. Funct. Mater.* **2003**, *13*, No. 9, September

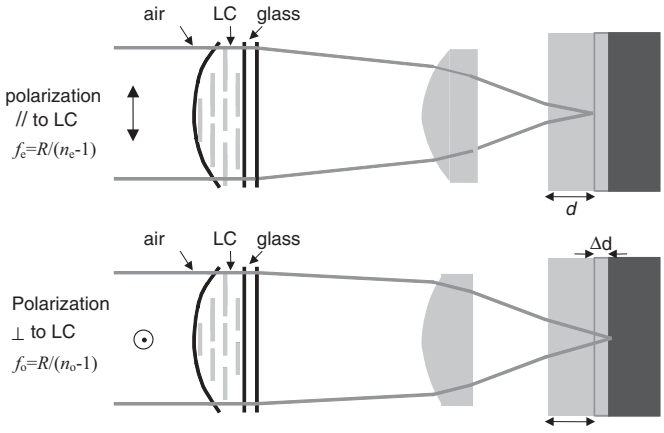

Fig. 1. Polarization-sensitive lens ($n_e > n_o$).

lens. The vergence can be switched between two states using the two polarization modes of the PS lens.

The bifocal nature of the LC lens can be used when the linear polarization can be rotated, for instance by a simple twisted nematic LC cell (TN cell) in combination with a polarizing beam splitter (PBS) and a quarter-wave ($\lambda/4$) plate, as shown in Figure 2. In the off-mode the TN cell rotates the polarization by 90°. As a result, the light rays interact with a medium which has a refractive index of n_0 and focus point f_0. While in the on

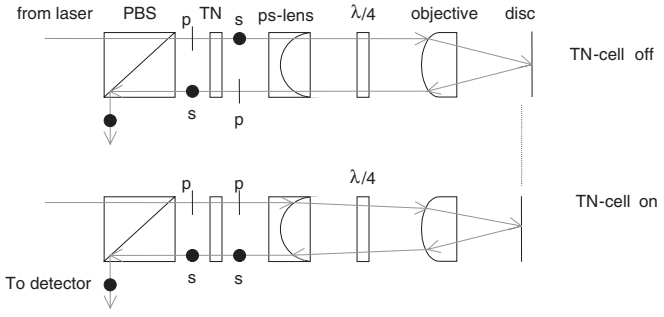

Fig. 2. Light path with LC lens.

mode, when the polarization direction is not rotated, the light rays interact with a medium which has a refractive index n_e and a corresponding focus point f_e. Hence, the introduction of a TN cell enables the use of the PS lens as a binary switchable lens. The additional quarter wave plate has two functions. Firstly, the linear polarization of the light coming from the TN cell is converted to circular polarization. The sensitivity for birefringence in the top layer of the disc thereby decreases. Secondly, after reflection from the disc, the handedness of the circular polarization is reversed. When this opposite handedness travels through the quarter wave plate again, the linear polarization has changed by 90°. In this way, the combination with the TN cell always ensures s-polarized light which is then reflected from the PBS and prevents the light from re-entering the laser.

The main objective of this paper is to describe the successive photoreplication[12] of anisotropic lenses made from a single mold (as outlined in the Experimental section; see Fig. 9), and the characterization of the optical properties of the components obtained. For this purpose, mixtures of an LC diacrylate and a non-reactive LC—a cyanobiphenyl mixture with a small portion of a cyanoterphenyl compound (E7)—were prepared. E7 was used to tune the refractive indices and to match them to the glass support. An extra advantage of using a non-reactive species as an additive is the reduced polymerization shrinkage. The polymerization kinetics, the birefringence, and the alignment of the LC mixtures were characterized. Finally, LC lenses were fabricated using the proprietary photoreplication process, as well as by filling a small semi-spherical cavity between glass plates.

2. Results and Discussion

2.1. Phase Diagram

1,4-Di(4-(3-acryloyloxypropyloxy)benzoyloxy)-2-methylbenzene (RM257) is an LC diacrylate with a nematic phase between its melting point at 70 °C and its clearing point at 130 °C. E7, an LC mixture derived from cyanobiphenyls, was used to increase the refractive indices and the birefringence of the mixtures, and to suppress crystallization of RM257 at room temperature. E7 exhibits a nematic phase between –20 °C and +55 °C. The phase diagram of the RM257/E7 mixtures was obtained using differential scanning calorimetry (DSC) and is given in Figure 3. The nematic to isotropic transition temperatures of the mixtures decrease with the increasing E7 content

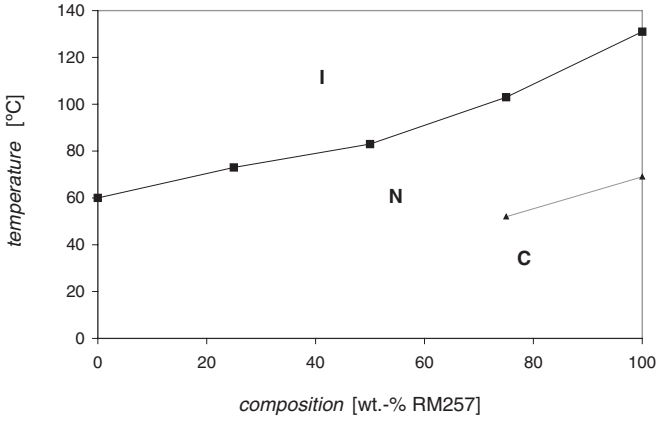

Fig. 3. Phase diagram of binary mixtures of RM257 and E7. ◆ $T_{melting}$; ■ $T_{clearing}$.

due to the lower isotropic transition temperature of E7 compared to RM257. All mixtures remain nematic upon heating and only one clearing point was observed. We can therefore conclude that the system is miscible in the nematic phase. Only the mixtures 100:0 [wt.-%] and 75:25 [wt.-%] crystallize slowly within a day at room temperature.

2.2. Photopolymerization

The conversion of RM257 as measured both by DSC and Fourier-transform infrared (FTIR) spectroscopy depends on

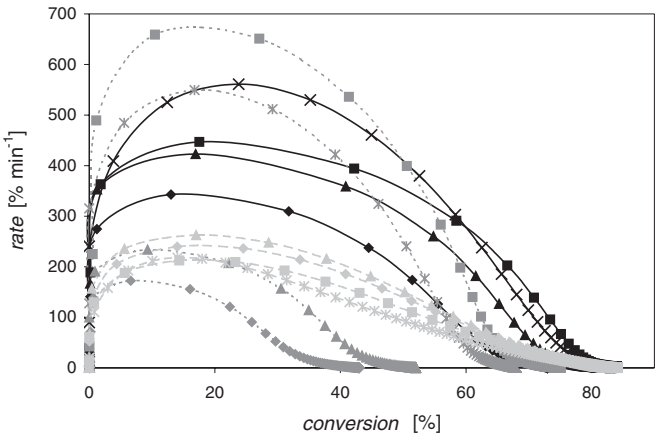

Fig. 4. Rate of polymerization as a function of the conversion for various RM257/E7 mixtures. ◆ 40 °C; ▲ 60 °C; ■ 80 °C; × 100 °C. - - - - - 100:0; — 75:25; – – – 25:75 [wt.-%].

the polymerization temperature, with a maximum at around 80 °C. Interestingly enough, the polymerization temperature did not have much influence on the conversion of the different mixtures: conversions were somewhere between 75 % and 85 % complete after less than 10 min of irradiation with 7 mW cm^{-2} under the same conditions.

Figure 4 compares the polymerization rate as a function of conversion and temperature for the different mixtures. Immediately after the start of the polymerization, gelation causes auto-acceleration, and the rate of polymerization increases rapidly to a maximum which is a function of temperature and the LC mixture.[13] Upon further polymerization, monomer depletion and mobility effects cause a decrease in the polymerization rate.

It is interesting to note that the polymerization rate for all mixtures containing E7 was no longer detectable at around 75–85 % conversion for all polymerization temperatures. However, the conversion at the near-zero rate of polymerization of RM257 decreases with the decreasing temperature (to 40 % at $T = 40$ °C), as shown in Figure 4. The difference between RM257 and the mixtures may be due to later vitrification and higher monomer mobility in the mixtures. The minimal difference in conversion between the various mixture compositions means that network mobility is increased significantly with relatively small amounts of non-reactive compounds.

We observed a maximum in the rate of conversion close to 80 °C for the pure compound, which agrees with values reported by others.[13–15] The rate of polymerization in the various mixtures decreases with the increasing amount of E7 as a result of dilution. We also found that the rate of conversion for a given mixture increases with an increasing temperature, as long as the mixture is still in the nematic phase. In the isotropic state, the polymerization rate as a function of the conversion decreases with an increasing temperature (see Fig. 4, 25:75 [wt.-%] 60 °C, 80 °C, and 100 °C, for example).

Hikmet[13] reported similar behavior for pure compounds. The temperature dependence of the rate of polymerization for polymeric networks is however extremely complex and allows only a qualitative comparison with previous work. An explanation that is sometimes used for decreasing polymerization rates at higher temperatures is that disproportionation becomes more important at higher temperatures.[16] Increased disproportionation cannot explain our results with the RM257/E7 mixtures, since the phenomenon already occurs at low temperatures for the 25:75 mixture.

No clear relationship between the nematic to isotropic transition and the rate of polymerization has been observed before, but there are indications that the molecular order affects termination and free-radical transfer reactions. Evidence of such effects may be found in the fact that in the isotropic state, the gelation point and vitrification are reached at lower conversion percentage. This can be determined qualitatively from the curves of Figure 4, as the maximum polymerization rate shifts to higher conversions in the nematic state, but decreases when the nematic to isotropic transition temperature has been passed. The maximum polymerization rate is believed to be related to the gelation and vitrification of the network, thus reducing monomer mobility.[12,17]

2.3. Birefringence

The birefringence of the polymerized RM257 mixtures with increasing E7 concentration was measured as a function of temperature, both during heating and cooling scans. The birefringence of RM257 polymerized at 80 °C, at 60 °C and at 40 °C is represented in Figure 5. We observed a large difference in birefringence between the first heating and cooling runs for the samples. This difference was not found in the second heating run. During the first heating cycle RM257 reached almost complete conversion by thermal polymerization; the birefringence remains constant from about 120 °C. Figure 6 shows the birefringence of the 75:25 wt.-% RM257/E7 mixture during cooling. The values obtained in the second heating run were the same as in the cooling run. In contrast to pure RM257, the polymerization temperature hardly influenced the birefringence of the obtained network, as can be seen from the minor differences between the three temperatures of polymerization.

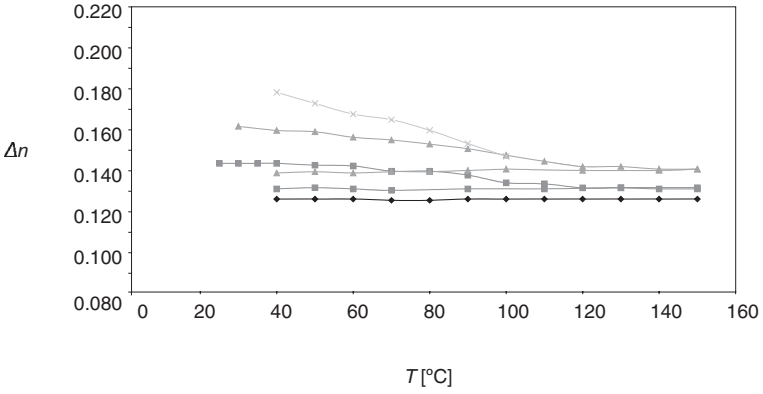

Fig. 5. Birefringence as a function of temperature for monomer and RM257 networks polymerized at different temperatures. Average values of $\lambda = 480$, 546, and 589 nm. ▲ 40 °C (heating and cooling scan); ■ 60 °C (heating and cooling scan); ◆ 80 °C; × monomer.

ADVANCED FUNCTIONAL MATERIALS

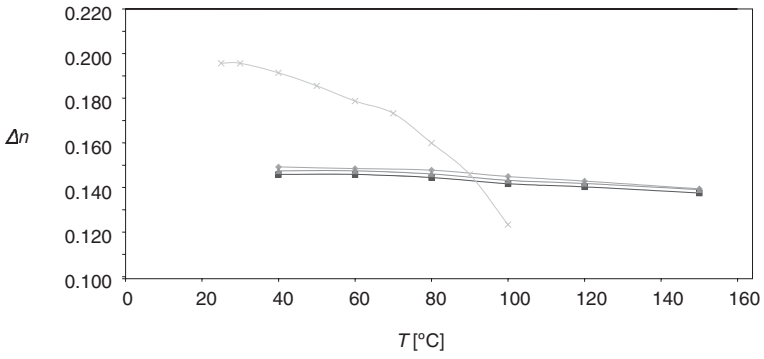

Fig. 6. Birefringence as a function of temperature for 75:25 wt.-% RM257/E7 polymerized at different temperatures. Average values of $\lambda = 480$, 546, and 589 nm. ◆ 20 °C; ■ 40 °C; ▲ 60 °C; × monomer mixture.

The loss of order for RM257/E7 75:25 [wt.-%] is probably less than for the pure diacrylate due to the fact that 25 % of the material is not linked to the polymer and therefore remains oriented. The addition of a small amount of mobile LC monomer to the network consequently decreases the effect of orientational loss during polymerization at elevated temperatures. For 50:50 [wt.-%] RM257/E7 networks an increase in temperature lead to a large decrease in residual birefringence for all polymerization temperatures studied. This is in contrast to 100:0 [wt.-%] and 75:25 [wt.-%] RM257/E7 networks, where a very stable birefringence as a function of temperature was found. We attribute this behavior to E7 that is partially bonded to the network and partially free inside the network.[16] The non-bonded E7 loses order due to isotropisation at around 60 °C, which is consistent with the fast decrease of the birefringence found in the 50:50 [wt.-%] mixture.

2.4. LC Lenses Obtained by Filling a Curved Mold: Comparison of Rubbed and Photoaligned Devices

RM257, E7, and the RM257/E7 mixtures form a monodomain with good planar alignment in a 3 cm^2 cell provided with rubbed AL-1051 or AL-3046 polyimide films. The measured twist angle corresponds to the twist of 60 ° enforced by the two polyimide layers, indicating that the anchoring is comparable. The polyimide photoalignment material RN-1349 showed identical results.

We next studied the alignment of LC mixtures in a small semi-spherical cavity made in glass. After filling the pit with LC material a second thin glass plate was put on top, resulting in a small lens on which optical measurements were performed. We compared lenses with induced orientation by mechanical rubbing using AL-1051, and photoalignment using RN-1349. Lenses were made using 50:50 [wt.-%] RM 257/E7. Although this mixture does not show stable birefringence over a broad temperature range, it does not crystallize during application and its refractive indices match well with the glass.

Figure 7 shows the interferograms of the extraordinary mode for two lenses. The ordinary refractive indices are well matched with the glass substrates. We found only small differences in the interferograms of the extraordinary modes of the lenses obtained by mechanical rubbing and those made by photoalignment. For this mode one or two more fringes were found for the mechanically rubbed LC lens indicating a higher n_e and thus a larger effective birefringence.

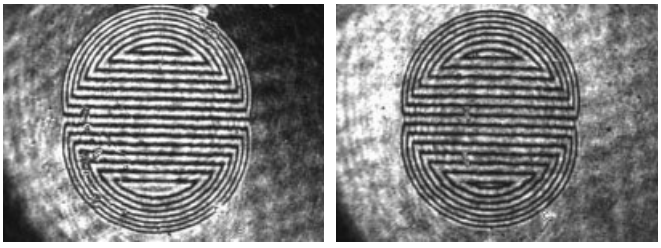

Fig. 7. Shearing interferograms for the extraordinary mode of LC lenses from polymerized 50:50 wt.-% RM 257/E7 with alignment induced by mechanical rubbing (left) or by photoalignment (right).

The slightly lower lens power of photoaligned lenses is attributed to a small tilt of the LC molecules on RN1349. Nevertheless, the total rms of wavefront aberrations of both lenses shown in Figure 7 is between 20 and 30 mλ. The astigmatism of these lenses is within the noise of the measured wavefront aberration level.

2.5. Optical Properties of Anisotropic Lenses Obtained by Lens Replication

The 75:25 [wt.-%] RM257/E7 mixture is very suitable for photoreplication, as it combines a relatively high and stable birefringence, good alignment properties, a broad nematic phase, and almost temperature-independent high conversions and birefringence after photopolymerization. The combination of AL1051 on the curved glass mold and the reactive polyimide ZLI 2650 on the flat substrate also aligned the RM257/E7 75:25 [wt.-%] mixture very successfully, as can be concluded from a distinct color change which is observed when the sample is moved from 0° to 45° under crossed polarizers. No change in the alignment was noted after polymerization. The methacrylate groups present in ZLI 2650 react with the acrylate groups in the LC mixture upon irradiation, thereby providing adhesion to the flat substrate. A surfactant can be added to the mixture to further improve release properties from the mold. However, the value of the measured effective birefringence changes significantly when a surfactant is added, which decreases the nematic-to-isotropic transition temperature. For example, in a lens where $R = 100$ mm, the $\Delta n_{eff} = 0.1586$ without surfactant

and $\Delta n_{\text{eff}} = 0.1458$ with surfactant (see Table 1). In general, multiple replicas could be made from all molds used. Optical properties of the lenses were measured using shearing interferometry. The aberrations, the focal lengths of both the extraordinary and the ordinary refraction modes, and the refraction indices were calculated from the wavefront images. Table 1 shows the optical measurements of typical replicas.

The birefringence values found for all lenses are very close to those presented in Figure 6, although the calculated values for n_o and n_e may vary per lens type, which may be due to the deviation between the actual lens curvature and the mold curvature used in the calculation.

In the extraction of the Zernike aberration coefficients from the measured shearing interferograms, the radius of this measurement circle was set to a value between 80 % and 100 % of the pupil radius, depending on the presence of defects or an abnormally high curvature near the rim of the pupil.

The rms aberration level was below 20 mλ for most lenses, which is a requirement for practical applications. The largest aberration was usually astigmatism.[11] In principle, astigmatism in LC lenses cannot be eliminated completely. This is due to the curvature of the cavity region, which causes a rotation of the LC director field with respect to the polarization direction.

We can estimate the order of magnitude of the astigmatic aberration as it scales with $(d\,\Delta n/\lambda)\,NA^2$.[11] In the worst case we use the smallest curvature radius $R = 21$ mm and a birefringence value $\Delta n_{\text{eff}} = 0.15$. With a pupil radius of $a = 1.75$ mm, the numerical aperture is $NA = a/f = 1.75/42 = 0.042$. The lens thickness d is at least $a^2\,(2\text{R})^{-1} \approx 88\,\mu\text{m}$. With the wavelength $\lambda = 430$ nm it then follows that, in the worst case, $(d\Delta n/\lambda)\,NA^2 \approx 54$ mλ. Consequently, the measured astigmatism can be attributed to the birefringent nature of the LC lens. We suspect that the measured astigmatism is also influenced by polymerization shrinkage which affects the shape of the replicated lens. Shrinkage effects become more important with a smaller curvature radius and higher aspect ratios. Other possible contributions to measured aberrations are a small misalignment of the reference lens, and the used measurement area.

The lenses made with the mold with a curvature radius of 21 mm have very high aberrations. The shearing interferograms show the typical pattern which is associated with spherical aberrations (Fig. 8a). This could be due to the larger thickness variation between the flat zone and the lens area, which makes these lenses highly susceptible to polymerization shrinkage variations as a function of the lens radius.[17] The lens shape will then be less accurately replicated resulting in an increase of spherical aberrations.

The rms aberration values of the lenses made from the mold with a radius of 100 mm are generally below 20 mλ when the radius of the measurement circle is set at 80 % of the pupil radius. There is a high increase of the aberration coefficients when the calculations are performed on the total lens aperture, as can clearly be seen in the interferogram of Figure 8b. There seems to be a small distortion of the LC orientation at the mold border, which can be attributed to the difference between the tilt angle of the oriented polyimide and the mold curvature.

The measurements show that the lenses made from the mold with a radius of 49 mm have the best optical properties. Figure 8c shows a typical lens with $R = 49$ mm, indicating a very homogeneous LC orientation, including the regions near the pupil borders. The total rms aberration is generally below 20 mλ when the radius of the measurement circle is equal to the pupil radius.

When extra functionality is desired, active components can also be of interest. These components combine the voltage induced switching properties of LC materials with a lens function. This subject will be the topic of an forthcoming paper.

3. Conclusion

We have described the first successful replication of anisotropic lenses from molds with different curvatures. The optical aberrations of the LC replicas were small, typically with rms values below 20 mλ (at 430 nm).

Table 1. Optical properties measured at 430 nm of different replicas using 75:25 wt.-% RM257/E7.

Radius [mm]	Polarization	Pupil area [%]	RMS [mλ]	RMS Astigmatism [mλ]	RMS Spherical aberration [mλ]	Focal length [mm]	Refractive indices[a]	Comments
21	e	80	150.6	30.4	145.7	35	1.6000	with surfactant
21	e	100	279.6	34.0	269.4			
21	o	80	118.2	9.1	113.8	45	1.4667	
21	o	100	212.6	23.6	200.7			
49	e	80	13.3	7.4	6.8	70	1.7000	with surfactant
49	e	100	20.4	9.0	10.0			
49	o	80	7.0	3.5	1.2	89	1.5506	
49	o	100	7.7	4.0	0.5			
100	e	80	12.4	2.6	7.5	150	1.6667	with surfactant
100	e	100	105.0	18.7	80.9			
100	o	80	16.2	6.4	9.5	192	1.5208	
100	o	100	84.4	8.3	65.4			

[a] calculated using $f_{o,e} = R/(n_{o,e}-1)$ where R is the curvature radius of the mold cavity.

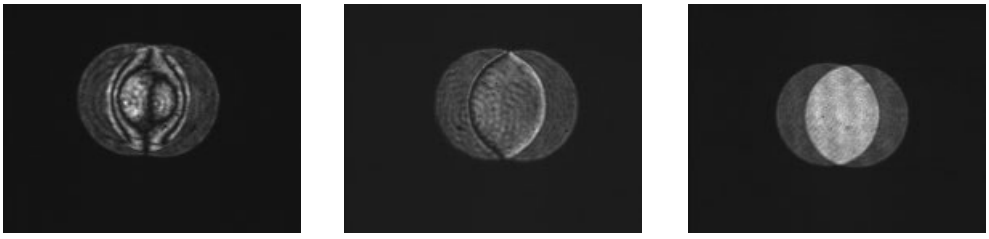

Fig. 8. Left: interferogram of a lens with a radius of 21 mm. Center: lens with a radius of 100 mm. Right: lens with a radius of 49 mm. The extraordinary modes are shown.

Focal lengths for the ordinary and extraordinary modes can be varied by the mold curvature and refractive indices of the LC mixture, thus enabling the fine tuning of parameters necessary for a specific application. The mixture with 25 [wt.-%] E7 has fast polymerization kinetics, favorable birefringence, good alignment properties, a broad nematic phase, and almost temperature-independent high conversions and birefringence after photopolymerization. Such passive LC lenses may find an application in light paths for spherical aberration correction, compensation devices for dual- (or multiple-) layer optical storage, or in multi-focal camera modules for mobile phones, among others.

4. Experimental

4.1. Materials

RM 257 was obtained from Merck. Gel particles were eliminated by dissolving the material in dichloromethane (1:1 wt./wt.), filtering over a 0.2 μm filter, and evaporating the dichloromethane. E7 (a cyanobiphenyl mixture with a small portion of a cyanoterphenyl compound) was obtained from Merck. Irgacure 651 (Ciba Geigy) was used as the photoinitiator.

The following polyimides were used for alignment: Precursor OPTMER AL-1051 and AL-3046 supplied by Japan Synthetic Rubber Co.; Merck ZLI-2650, a reactive polyimide with methacrylate groups; RN-1349 (Nissan Chemicals) a polyimide which can be photoaligned by photodegradation.

FC171, a perfluorinated surfactant (3M), and 2-(*N*-ethylperfluorooctane)sulfonamidoethylacrylate (Acros) were used as miscible surfactants for the promotion of lens release from the molds.

4.2. Methods

DSC. Sample quantities were heated to 140 °C and, after a 5 min hold, cooled to −20 °C using a Perkin–Elmer DSC-7 apparatus. A second heating curve was then recorded. Heating and cooling rates were 10 °C min^{-1}. The measurements were conducted under a constant N_2 flow of 50 mL min^{-1}. The phase diagram of the RM257/E7 mixtures was determined from the observed phase transitions in the temperature scans.

Photo-DSC. To follow the heat of the photopolymerization reaction, a Perkin–Elmer DSC-7 apparatus was used, adapted for illumination with a UV lamp (Philips PL10W) with a standard intensity of 7 mW cm^{-2} in the wavelengths from 340 to 410 nm. The photopolymerization experiments were performed using the initiator Irgacure 651 at a concentration of 2.5 wt.-%. Samples were illuminated for 20 min.

To remain within the heat probing capacity of the apparatus and to avoid an intensity gradient due to loss of UV by absorbance of the photoinitiator, small sample quantities (in the order of 1.5 mg, which gives a layer thickness of ~ 75 μm in the pans) were used, and the UV intensity was decreased by using a UV filter from Kodak (Nominal Density 0.9) with a measured transmission of 5.6 % in the desired wavelength range of exposure. The measurements were conducted under a constant N_2 flow of 50 mL min^{-1}. To mix the LC materials, the mixtures were heated to 105 °C and cooled at a rate of 5 °C min^{-1} to the temperature of polymerization. No conversion was observed in the DSC by heating samples in the dark. The conversion is calculated from the integrated area of the measurement, the molecular weight of the polymerizable molecule, and the heat of polymerization (ΔH) of the acrylate group of which two are present in the molecule; $\Delta H = 78$ kJ mol^{-1} [18].

FTIR. FTIR spectra were recorded on an ATI Mattson Genesis II FTIR spectrometer equipped with an attenuated total reflection (ATR), which can be used to obtain the infrared spectra of solids, including thin films. To prevent possible deviations by continued polymerization in the dark, the infrared spectra of the photopolymerized samples of the DSC were taken just after carrying out the photo-DSC experiment. The absorption band of the C–H out-of-plane vibrations of the acrylate group at approximately 810 cm^{-1} was measured relative to the absorbance of the C=O stretch-vibration absorption band of the mesogenic and acrylate ester groups at 1710 cm^{-1}, which we used as our internal standard. At total conversion the 810 cm^{-1} band had disappeared completely. A non-polymerized sample was measured in the same cups as the ones used in the photo-DSC experiments, for reference purposes.

Birefringence Measurements. Glass cells with a gap of approximately 5 μm were used. The internal cell surfaces were coated with thin layers of polyimide, which had been rubbed to induce homogeneous uniaxial orientation of the LC material. The thickness of the cell was measured via interference of an empty cell using a UV-vis spectrometer. The glass cells were filled by capillary suction. Birefringence measurements were carried out using a polarizing microscope equipped with an optical compensator (Leitz Tilting Compensator 1942 K) and a Mettler Toledo FP5 hot stage. The optical compensator was placed perpendicularly to the orientation axis of the LC material. The retardation (r) was measured as an average value of the retardation at 480, 546, and 589 nm. The birefringences before and after polymerization were measured as a function of temperature. Before polymerization the temperature range used was between 25 °C and 100 °C. Photopolymerization was performed at various temperatures. The Δn was then measured from 25 °C to 150 °C followed by a measurement from 150 °C to 40 °C.

Spin-Coating of Alignment Materials. AL1051 was spin-coated onto the glass molds. Reactive polyimides were spin-coated onto the flat substrates of the lenses to improve the release from the mold by ensuring that the LC material was chemically bonded to the flat substrate. The photoalignment materials were spin-coated onto flat glass substrates to test their alignment power.

Alignment of Reactive Mesogens and Mixtures on Rubbed and Photoaligned Films. To determine their ability to form a monodomain and to test the anchoring properties, the alignment power of the alignment materials, AL-1051, AL-3046, and RN-1349 was tested by fabricating cells, with a 6 μm cell gap and an area of 3 cm^2, that were rubbed anti-parallel or 60° twisted. A qualitative measure for the anchoring properties is the deviation of the actual twist from the forced twist [15]. The twisted cells were analyzed on their actual twist angle by means of visible spectroscopy (Perkin–Elmer Lambda 800 UV-vis spectrometer) [19]. One substrate of the twisted cells was supplied with a rubbed AL-1051 layer, assumed to have 'infinitely' high anchoring. The substrates of the anti-parallel cells consisted of identical alignment layers. For the photoalignment material RN-1349, an Ushio UX-1000SM-AHG01 Projection Exposure System was used to create the chemical anisotropy at the surface. Finally, the cells were capillary filled at 80 °C with a melt of the mixtures, and subsequently exposed to 365 nm UV light (PLS10) for 30 min to crosslink the reactive mixture. Pure RM257 and a 75:25 wt.-% RM257/E7 mixture were investigated for monodomain formation and anchoring ability.

Lens Replication. This process is schematically outlined in Figure 9. A semi-spherical cavity with curvature radius R was machined in a flat 3 mm thick plate of glass. The diameter (d) was 3.5 mm and the depth of the cavity in the center was h. A thin layer (< 100 nm) of alignment material was applied by spin-coating. The cured alignment layer was subsequently treated by rubbing or photoalignment to create chemical and/or geometrical anisotropy, to which the director of the reactive LC material is sensitive.

A droplet of isotropic LC was put carefully (in order to avoid the inclusion of air bubbles) in the spherical cavity which was heated at 80 °C. A 1 mm thick flat glass substrate was applied on top with the alignment direction anti-parallel to that of the mold (Fig. 9c). In order to achieve a homogenous thin LC layer, a weight was put on the glass; weights of 600 g and 250 g were used. The lens sam-

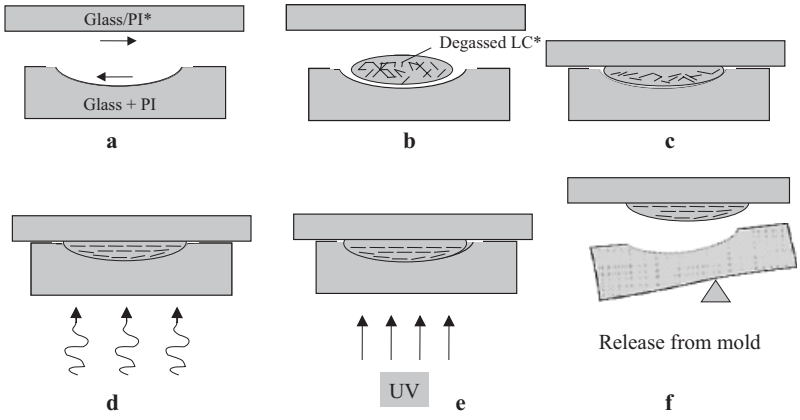

Fig. 9. Photoreplication steps (see text for explanation).

ple was cooled to room temperature in 30 min during which time the LC became nematic.

When multi-domains appeared at this stage, the LC mixture was heated for 3 min to 105 °C (which is above the clearing point), to destroy the multi-domain orientation. It was subsequently cooled to obtain a homogeneous orientation (Fig. 9d). The mixture was finally polymerized using UV light intensities of 10 mW cm^{-2} for 60 s (Fig. 9e). We checked the uniformity of the LC alignment using a light microscope.

To release the lens from the mold, the flat substrate was pressed against a flat support with one of the corners outside of the support. Force was applied to the free corner to bend the flat substrate. The glass mold was then separated from the lens and could be reused (Fig. 9f).

Three different molds were used in order to characterize the influence of the mold parameters on the optical properties of the lenses. The geometrical parameters are given in Scheme 1.

Shearing Interferometry. The optical performance of the lenses was measured using shearing interferometry [20]. A parallel beam of coherent light passed a

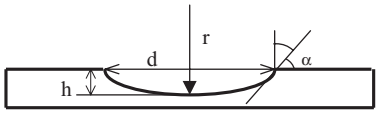

r = curvature radius
d = diameter
h = height
α = angle between the tangent and mold surface.

r [mm]	d [mm]	h[mm]	α[°]
100	3.36	0.014	0.96
49	3.44	0.030	1.97
21	3.84	0.088	5.50

Scheme 1. Geometrical parameters of the glass molds used.

telescope consisting of an off-the-shelf Spindler & Hoyer lens and the LC lens. It then passed two binary gratings, which are designed so that all light is diffracted into the –1st and +1st diffraction orders. In this way, the beam was split into two mutually displaced parallel beams. The interference pattern in the region where the two sub-beams overlap, was imaged onto a charge coupled device (CCD) camera. During measurements the gratings are displaced with respect to each other by a piezo-element in a number of steps. The five-step algorithm described in [20] was used. The interference patterns measured after each step were registered by the computer which then extracted the wavefront aberration. According to Zernike's theory [20], the wavefront aberration can be decomposed into an orthogonal set of aberrations. The coefficients of the decomposition are called Zernike coefficients (in m$\lambda = \lambda/1000$), and are a convenient measure for the size of the different aberrations.

Received: March 28, 2003
Final version: June 23, 2003

[1] M. Kuijper, I. P. Ubbens, L. Spruijt, J. M. ter Meulen, K. Schep, *Proc. SPIE—Int. Soc. Opt. Eng.* **2001**, *4342*, 178.
[2] H. Ogawa, *Technical Digest of the International Symposium on Optical Memory* **2001**, *6*, 2001.
[3] J. Braat, *Appl. Opt.* **1997**, *36*, 8459.
[4] M. Born, E. Wolf, *Principles of Optics*, 6th ed., Cambridge University Press, Cambridge, UK **1980**.
[5] Y. Tsuchiya, S. Kajiyama, Y. Kano, Y. Matsumura, S. Ichiura, *Jpn. J. Appl. Phys.* **1997**, *36*, 481.
[6] Y. Tanaka, M. Yamagata, Y. Komma, S. Mizuno, K. Nagashima, *Jpn. J. Appl. Phys.* **1998**, *37*, 2179.
[7] Y. Komma, K. Kasazumi, S. Nakano, S. Mizuno, *Proc. SPIE—Int. Soc. Opt. Eng.* **1994**, *2338*, 282.
[8] S. Sato, T. Nose, *Proc. SPIE—Int. Soc. Opt. Eng.* **1999**, *3800*, 72.
[9] M. Honma, T. Nose, S. Sato, *Opt. Rev.* **1999**, *6*, 139.
[10] S. Sato, *Jpn. J. Appl. Phys.* **1979**, *18*, 1679.
[11] S. Stallinga, J. Vrehen, J. Wals, H. Stapert, E. Verstegen, *Proc. SPIE—Int. Soc. Opt. Eng.* **2000**, *4081*, 50.
[12] J. G. Kloosterboer, *Adv. Polym. Sci.* **1988**, *84*, 1-16.
[13] R. A. M. Hikmet, *Liq. Cryst.* **1991**, *9*, 405.
[14] D. Andrienko, Y. Kurioz, M. Nishiwaka, Y. Rexnikov, J. L. West, *Jpn. J. Appl. Phys.* **2000**, *39*, 1217.
[15] S. T. Tang, H. S. Kwok, *J. Appl. Phys.* **2000**, *89*, 80.
[16] R. A. M. Hikmet, J. Lub, *Prog. Polym. Sci.* **1993**, *21*, 1165.
[17] E. J. K. Verstegen, J. Faasen, H. R. Stapert, P. Duineveld, J. G. Kloosterboer, *J. Appl. Polym. Sci.*, in press.
[18] J. Leonard, in *Polymer Handbook*, 4th ed. (Eds: J. Brandrup, E. H. Immergut, E. A. Grulke), Wiley-VCH, Weinheim **1975**, Ch. 2.
[19] D. J. Broer, J. Lub, C. F. van Nostrum, M. M. Wienk, *Recent Res. Dev. Polym. Sci.* **1998**, *2*, 313.
[20] D. Malacara, *Optical Shop Testing*, Wiley-Interscience, New York **1992**.

